Title: Kv1.1 channelopathy abolishes presynaptic spike width modulation by subthreshold somatic depolarization

Short title: Kv1.1 mutation abolishes presynaptic analog signaling

Umesh Vivekananda[1], Pavel Novak[2], Oscar D Bello[1], Yuri Korchev[3], Shyam S Krishnakumar[1,4], Kirill E Volynski[1] and Dimitri M Kullmann[1*]

[1]UCL Institute of Neurology, University College London, Queen Square, London, WC1N 3BG, United Kingdom

[2]School of Engineering and Materials Science, Queen Mary University of London, Mile End Rd, London E1 4NS, United Kingdom

[3]Department of Medicine, Imperial College London, London, Du Cane Road, London W12 0NN, United Kingdom

[4]Department of Cell Biology, Yale University School of Medicine, New Haven, Connecticut 06510, United States.

*Correspondence to: d.kullmann@ucl.ac.uk; Tel: +44 (0)20 3448 4100

Keyword: Channelopathy, synaptic transmission, potassium channel

Abstract

Although action potentials propagate along axons in an all-or-none manner, subthreshold membrane potential fluctuations at the soma affect neurotransmitter release from synaptic boutons. An important mechanism underlying analog-digital modulation is depolarization-mediated inactivation of presynaptic Kv1-family potassium channels, leading to action potential broadening and increased calcium influx. Previous studies have relied heavily on recordings from blebs formed after axon transection, which may exaggerate the passive propagation of somatic depolarization. We recorded instead from small boutons supplied by intact axons identified with scanning ion conductance microscopy in primary hippocampal cultures, and asked how distinct potassium channels interact in determining the basal spike width and its modulation by subthreshold somatic depolarization. Pharmacological or genetic deletion of Kv1.1 broadened presynaptic spikes without preventing further prolongation by brief depolarizing somatic prepulses. A heterozygous mouse model of Episodic Ataxia type 1 harboring a dominant Kv1.1 mutation had a similar broadening effect on basal spike shape as deletion of Kv1.1; however, spike modulation by somatic prepulses was abolished. These results argue that the Kv1.1 subunit is not necessary for subthreshold modulation of spike width. However, a disease-associated mutant subunit prevents the interplay of analog and digital transmission, possibly by disrupting the normal stoichiometry of presynaptic potassium channels.

Significance statement

Synaptic transmission depends on all-or-none action potentials. However, subthreshold membrane potential fluctuations at the cell body spread passively along the axon and affect the

shape of presynaptic action potentials, calcium influx and neurotransmitter release. Here we apply a super-resolution method to identify small presynaptic terminals for patch clamp. Subthreshold modulation of action potentials is abolished by a mutation in the potassium channel Kv1.1 associated with the neurological channelopathy Episodic Ataxia type 1. Surprisingly, pharmacological or genetic ablation of Kv1.1 fails to prevent subthreshold modulation. Kv1.1 deletion and mutation have distinct effects on the composition and voltage sensitivity of presynaptic channels and consequently on modulation of neurotransmitter release.

\body

Introduction

Although action potentials are generated at the axon initial segment in an all-or-none manner, synaptic transmission can be modulated by electrotonic propagation of subthreshold membrane depolarization from the soma (1–6). Inactivation of axonal Kv1 family channels contributes to 'analog' signaling by broadening presynaptic action potentials (6–9). Investigations of presynaptic spike shape in small presynaptic boutons have relied heavily on extrapolation from recordings in blebs that form after axons have been transected (2, 6, 8, 9). A potential pitfall of this method is that the ion channels present in blebs may not be representative of the normal complement of channels at an unperturbed bouton. A further difficulty is that the attenuation of voltage with distance from the soma is likely to be smaller than when recording from an intact axon. Indeed, classical cable theory predicts that steady-state somatic voltage should decrease by approximately 63% at one length constant if the axon is represented by an infinite cable, but only by ~35% if it is sealed at the same point (10). The discrepancy increases as the axon is made shorter: if the axon is cut at half a length constant, the attenuation of steady-state voltage at its termination is only ~29% of that predicted for an infinite cable. Given that the length constant of unmyelinated axons in the CNS has been estimated in the range of 400 – 600 μm (1–3, 9, 11), this implies that the modulation of action potential shape by passively propagating subthreshold somatic depolarization may have been greatly overestimated.

Recordings from large mossy fiber boutons avoid the pitfalls of recording from axon blebs. However, although presynaptic depolarization broadened spikes and action-potential evoked Ca^{2+} transients in one study (12), this was not detected in other studies which examined sub-threshold depolarization propagating from the soma (1, 3). Presynaptic recordings from calyceal synapses in the brainstem, furthermore, detected an increase in Ca^{2+} transients without change in spike shape upon depolarization, whether elicited by activation of presynaptic glycine

receptors (13) or by direct current injection (14). The principles governing analog-digital modulation at large calyceal synapses may not, however, apply to far more abundant small presynaptic boutons of the forebrain, arguing the need for alternative recording methods to resolve the role of spike broadening. Presynaptic voltage-sensitive fluorescence measurements or loose patch clamp of fluorescent-dye loaded axons may not detect sub-millisecond differences in action potential shape.

To resolve the role of spike broadening by direct recording whilst avoiding the pitfalls of axon blebs, we used a variant of scanning ion conductance microscopy (hopping probe ion conductance microscopy – HPICM) (15) to identify small intact presynaptic boutons in mouse hippocampal cultures for patch clamp. We have previously reported that boutons thus identified express sodium, potassium and calcium channels (16), the full complement of channels required for action potential invasion and neurotransmitter release. We focus on the role of Kv1.1, a member of the Kv1 potassium channel family, which is expressed in the axons of pyramidal neurons (17). We show that action potential width recorded at the bouton is increased by relatively brief subthreshold depolarizing current injected at the soma of the same neuron. We further ask how Kv1.1 modulates spike shape, and identify an unexpected difference between the effects of pharmacological and genetic deletion of Kv1.1 on the one hand, and a dominant disease-associated missense mutation of the same subunit on the other.

Results

We first obtained a somatic whole-cell recording (**Fig. 1A**), and then used HPICM to obtain a high resolution 3D topographical image of a small region within 100 μm of the patched soma, looking for a candidate bouton for patch clamp (**Fig. 1B**). We applied the following criteria: first, the bouton should be situated on top of, or to one side of, a dendrite, and part of its surface

should be accessible to the vertical scanning nanopipette; second, axons connected to the bouton should be detected; and third, it should be clearly distinct from other neuronal structures. The scanning pipette tip was subsequently broken to widen its orifice by lowering it rapidly on an exposed region of the coverslip (16), before returning it to the identified bouton and obtaining a whole-cell patch clamp recording. In approximately 24% of cases action potentials elicited at the soma were detected at the bouton, confirming that both pipettes recorded from the same neuron (**Fig. 1C**). The red fluorescent tracer Alexa Fluor 568 routinely included in the bouton pipette labeled neighboring boutons either side of the targeted structure, providing morphological confirmation of the axon identity (**Fig. 1D**), and showing that the axon was not transected. The axon typically could not be traced back to the cell body because of its tortuous route. Nevertheless, the spike latency was non-significantly longer in the bouton than in the somatic recording (average ± SD soma-bouton difference: 0.02 ± 0.10 ms, n = 53), consistent with action potential initiation at the axon initial segment and a mean distance of 200 – 300 μm (9).

Of the Kv1 potassium channel family, Kv1.1 activates and, depending on co-assembled subunits, inactivates at relatively negative membrane potentials (18, 19). It is widely expressed throughout the CNS (20, 21), including the axons of pyramidal neurons (17), and is therefore a strong candidate to mediate the effect of subthreshold somatic de- and hyperpolarization on presynaptic spike shape. We asked if channels containing the Kv1.1 subunit affect spike width by examining the effect of acute application of the selective blocker Dendrotoxin-K (DTx-K, 20 nM) (22) on action potentials elicited by somatic depolarizing current pulses. The half-width of action potentials recorded at the soma was unaffected (**Fig. 2A** and **Fig. S1**). However, DTx-K application led to a 13 ± 3% (mean ± SEM) broadening of the action potential simultaneously recorded at the bouton (**Fig. 2A, B**) consistent with targeting of the channel to the axon.

We interleaved simultaneous somatic-bouton recordings in cultures obtained from wild type and *Kcna1*$^{-/-}$ mice lacking Kv1.1 (23). Although somatic action potential width was not significantly

different between genotypes, deletion of Kv1.1 broadened the presynaptic spike width by ~ 25% (*Kcna1*$^{-/-}$: 1.43 ± 0.1 ms, *n* = 9; WT: 1.12 ± 0.04 ms, *n* = 29; **Fig. S2A, B**). As expected, DTx-K had little or no effect on simultaneously recorded bouton or somatic spike width in *Kcna1*$^{-/-}$ neurons (**Fig. S2C, D**).

We compared the effect of pharmacological and genetic deletion of Kv1.1 to a mouse knock-in model of Episodic Ataxia type 1 (EA1), a channelopathy caused by heterozygous mutations in the Kv1.1-encoding gene *Kcna1* (24, 25). Kv1.1 co-assembles with other members of the Kv1 family, and several EA1-associated mutations exert a dominant negative effect on other K^+ channel subunits (26–28). The *Kcna1*$^{V408A/+}$ mouse model of EA1 (29) therefore allows the effect of disrupting the normal composition of heteromultimeric Kv1 channels to be studied. Similar to *Kcna1*$^{-/-}$ neurons, presynaptic spikes were 25% broader in neurons from *Kcna1*$^{V408A/+}$ than wild type mice (*Kcna1*$^{V408A/+}$: 1.40 ± 0.06 ms, *n* = 13; WT: 1.12 ± 0.04 ms, see above; **Fig. 2C**). Furthermore, as in *Kcna1*$^{-/-}$ neurons, DTx-K was ineffective in *Kcna1*$^{V408A/+}$ neurons, either in somatic (**Fig. 2D** and **Fig. S3**) or in bouton recordings (**Fig. 2D, E**).

Broadening of spike width by DTx-K in wild type neurons was also observed in experiments where a somatic recording was not obtained, and where action potentials were elicited by current injection at the bouton (**Fig. S4**). DTx-K also failed to broaden spikes in *Kcna1*$^{-/-}$ *and* *Kcna1*$^{V408A/+}$ boutons in this recording configuration, consistent with the results obtained with simultaneous soma-bouton recordings.

These data show directly that Kv1.1 affects spike shape at the bouton. To investigate the role of Kv1.1 in the interplay of analog and digital signaling we restricted our attention to neurons where paired somatic-bouton recordings were obtained. We examined the effect of injecting somatic currents ranging between –100 and +50 pA immediately before a supra-threshold somatic depolarizing current. Prepulses were 200 ms in duration, approximating the time course

of subthreshold excitatory postsynaptic potentials (1). No current was injected via the bouton pipette, thereby avoiding any errors arising from imperfect bridge balance.

In neurons from wild type mice the presynaptic action potential width showed a positive dependence on the pre-pulse, consistent with voltage-dependent inactivation of K^+ currents (**Fig. 3A**). This relationship persisted when spike width was plotted against the voltage of the bouton membrane prior to the somatic depolarizing pulse used to evoke spiking (**Fig. 3A**). In order to quantify this dependence, we calculated the Spearman rank correlation coefficient ρ between the pre-pulse current (or bouton voltage) and the spike width in each experiment. The null hypothesis that ρ should be randomly distributed around 0 was rejected at $p < 0.005$ ($n = 20$; Wilcoxon signed-rank test, **Fig. S5A**). In parallel, in order to compare across neurons, we normalized the half-width measured in each neuron by the average width measured with –100 and –50 pA prepulses (**Fig. 3B**, filled symbols). This showed a consistent upward-concave relationship. Spike broadening was not accompanied by a detectable change in spike height.

DTx-K had no significant effect on prepulse-dependent spike broadening ($n = 18$; dependence on pre-pulse current remained significant at $p<0.001$, Wilcoxon signed rank test; **Fig. 3B**, open symbols). The modulation of spike width by subthreshold pre-pulses was unaffected UK-78282 (200 nM), which has been reported to block Kv1.3 and Kv1.4 channels (30) (**Fig. S6**). Moreover, when the same protocol was repeated in neurons from *Kcna1*$^{-/-}$ mice, a positive relationship between spike width and prepulse amplitude persisted ($n = 9$; **Fig. 3C, Fig. S7**). These results indicate that, contrary to expectation, Kv1.1 is not necessary for digital-analog modulation.

In striking contrast to pharmacological or genetic deletion of Kv1.1, prepulses had no effect on spike width in *Kcna1*$^{V408A/+}$ neurons (**Fig. 4A, B**; $n = 10$; Wilcoxon signed-rank test for ρ versus somatic subthreshold current or bouton voltage: $p = 0.8$; **Fig. S5B**). The distributions of Spearman rank correlation coefficients in *Kcna1*$^{V408A/+}$ and wild type neurons were significantly

different ($p < 0.03$, Mann-Whitney U test). Moreover, the normalized spike widths at 0 or 50 pA were significantly different ($p = 0.05$ and 0.02, respectively, unpaired *t*-tests). The same conclusion held when *Kcna1*$^{V408A/+}$ neurons were compared only to wild type littermates ($n = 10$) recorded on the same days (normalized half-width for 0 and +50 pA prepulses: $p = 0.02$ and 0.01, respectively, **Fig. S8**). We further verified that the difference between wild type and *Kcna1*$^{V408A/+}$ neurons persisted when longer prepulses lasting two seconds were applied (9) (**Fig. S9**).

A possible explanation for the unexpected consequence of the heterozygous V408A mutation is that it alters the stoichiometry of Kv1 channels. We therefore asked if the relative abundance of different Kv1 subunits differs in cortical synaptosomes from adult wild type and *Kcna1*$^{V408A/+}$ mice. We concentrated on Kv1.1, Kv1.2, Kv1.3, Kv1.4 and Kv1.6, which are expressed in the CNS. None of the specific imunoreactive signals, normalized to the corresponding SNAP25 band intensity, differed significantly between wild type and *Kcna1*$^{V408A/+}$ mice, although there were non-significant trends for lower Kv1.3 and higher Kv1.6 (**Fig. S10**).

Discussion

The present study shows that brief subthreshold somatic depolarization robustly broadens presynaptic spikes in small boutons of untransected axons. The prepulses used here lasted either 200 ms or 2s, comparable to excitatory postsynaptic potentials propagating passively from the soma (1). The data thus fill a gap in the evidence that action potential width modulation by relatively brief subthreshold somatic depolarizations occurs in intact axons. At hippocampal mossy fiber synapses presynaptic spike broadening leads to a proportional increase in Ca^{2+} influx (31), and a similar principle underlies signaling at basket cell terminals in the cerebellar

cortex (32). Assuming a Ca^{2+} current cooperativity ~2 (33, 34), the ~12% analog spike broadening seen here (Fig. 3B) is predicted to increase neurotransmitter release by ~25%.

This study also reveals an unexpected dissociation between the effects of manipulating Kv1.1 on the basal presynaptic spike width and on the modulation of spike width by membrane potential changes propagating passively from the soma. Pharmacological blockade or homozygous deletion of Kv1.1 broadened the action potential recorded in boutons but did not prevent the effect of subthreshold prepulses. This argues that, despite its relatively negative activation and inactivation kinetics, Kv1.1 is not absolutely necessary for spike width modulation by prepulses lasting 200 ms. Subthreshold modulation of spike width also persisted in the presence of a blocker of Kv1.3 and Kv1.4 channels. A heterozygous missense mutation of the Kv1.1-encoding gene *Kcna1*, in contrast, completely abolished the effect of prepulses on spike width, even though the basal spike width was no greater than when Kv1.1 was deleted.

The results are particularly unexpected in the light of what is known of the functional consequences of the V408A mutation. In contrast to some EA1-associated mutations, the V408A mutation expressed in *Xenopus* oocytes has relatively subtle effect on current density, voltage threshold, activation kinetics and heterotetramerization (26, 28, 35–37). Furthermore the mutation paradoxically retards N-type inactivation, implying a gain of function that might offset a mild deleterious effect on channel function (38). Nevertheless, the mutation is embryonal-lethal in the homozygous state (29), unlike the homozygous null mutation which is compatible with survival to adulthood in mice (23). A possible explanation for the results is that *Xenopus* oocyte recordings underestimate the severity of the dominant negative effect of the V408A mutation, resulting in functional loss of a wide range of Kv1 channels. Nevertheless, quantitative immunoblotting failed to reveal a substantial change in the relative proportion of different members of the Kv1 family in cortical synaptosomes. Homozygous deletion of Kv1.1, in contrast, may lead to the formation of Kv1 channel stoichiometries that are able to substitute for

Kv1.1-containing heteromultimers. Such channels most likely have kinetics that are slower or require a larger depolarization to activate, explaining the prolongation of the spike width, and yet undergo a similar slow inactivation upon sustained depolarization, explaining the persistence of analog modulation of spike width.

Axonal Kv1 channels have also been implicated in shunting somatodendritic plateau potentials, thereby allowing attenuated spikes to repolarize fully and amplify as they propagate to the distal axon (39). This phenomenon has been studied with axon blebs and requires much larger depolarizations than the spike broadening studied here, although occurs with a similar timecourse. The dependence of shunting on activation, and spike broadening on inactivation, of voltage-gated channels hints at functional heterogeneity of axonal channels composed of different Kv1 subunits.

Episodic Ataxia type 1 is dominated by paroxysms of cerebellar incoordination and myokymia (25). These are most likely attributable to abnormal GABA release from cerebellar basket cells (29) and to motor axon hyperexcitability respectively (40), both sites where Kv1.1 is especially abundantly expressed (20, 21, 40). Indeed, presynaptic spike broadening has been demonstrated at these terminals in the *kcna1*$^{V408A/+}$ mouse (32). Nevertheless, epilepsy occurs in a high proportion of affected individuals (25, 27), implying a role in circuit excitability in the forebrain. Whether impairment of analog-digital modulation contributes to this feature of the disease remains to be determined.

Materials and methods

Neuronal Cultures and Recording Solutions

Kcna1$^{V408A/+}$ female mice were crossed with wild type C57/BL6 mice. Hippocampal neurons were isolated from P1–P2 mouse pups and cultured in Neurobasal-based medium either on an astrocyte feeder layer or on poly-D-lysine-treated coverslips. All recordings were conducted at ambient temperature (23°C–26°C) 12–19 days after plating. The standard extracellular solution used in all experiments contained 125 mM NaCl, 2.5 mM KCl, 2 mM $MgCl_2$, 2 mM $CaCl_2$, 30 mM glucose, 0.01 mM NBQX, 0.05 mM APV, and 25 mM HEPES (pH 7.4).

High-Resolution Scanning

Topographic images were obtained using a custom-modified HPICM sample scanner (ICNano-S, Ionscope) and custom software as described previously (16). The scan head was mounted on an inverted Olympus IX71 microscope, with the nanopipette held vertically. Alexa Fluor 568 epifluorescence images were obtained via a red long-pass dichroic mirror (560nm cut-off), 590nm – 660 nm emission filters, and 470 - 490 LED illumination (OptoLeED, Cairn Research), and collected using an Evolve 512 EM-CCD camera (Photometrics).

Fine-tipped nanopipettes, used both to probe the neuronal topography and to obtain patch-clamp recordings, were pulled from borosilicate glass (OD 1 mm, ID 0.5 mm, Sutter Instruments) using a laser puller (P-2000, Sutter Instruments). The pipette resistance was in the range of 80 – 110 MΩ, corresponding to an estimated inner tip diameter of 90 – 125 nm, prior to chopping for whole-bouton recordings. Nanopipettes were held in voltage-clamp mode with an Multiclamp 700B patch-clamp amplifier (Molecular Devices).

Whole-cell patch recordings

A soma was patched under light microscopy using a 3 – 5 MΩ conventional patch pipette filled with 130 mM K gluconate, 10 mM KOH-HEPES, 1 mM KOH-EGTA, 10 mM KCl, 4 mM Mg-ATP, 0.5 mM Na-GTP (pH 7.35 with KOH). The nanopipette used for HPICM contained the same internal solution supplemented with 200 μM Alexa Fluor 568 (Invitrogen). After obtaining a high-

resolution image of a candidate bouton, identified as above or adjacent to a dendrite and supplied by an axon, the nanopipette was broken on an area of bare coverslip as previously described (16). The widened pipette (resistance 30 – 45 MΩ, corresponding to an inner tip diameter of 300 – 450 nm) was returned to the bouton to obtain a whole-cell recording and switched to current clamp mode. In a subset of experiments where the soma and bouton were not from the same cell, presynaptic spike widths were recorded by injecting current into the bouton after balancing the bridge (Fig. S4). In all other cases spikes were evoked via the somatic pipette, and the bouton was recorded passively. Recordings were filtered at 5 kHz, digitized at 10 kHz and acquired and analyzed off-line with custom LabVIEW (National Instruments) software. Cells where action potentials did not exceed 0 mV were discarded. The spike take-off point was estimated from the peak of the 2nd time-derivative of voltage, and spike half-width was measured at the half-way voltage between take-off and peak. Where several spikes were elicited, only the first was analyzed. For experiments where a bouton recording was obtained without a somatic recording, spikes were elicited with a 10 ms, 50 pA current injection. To assess analog modulation 200 ms-long prepulses of amplitude –100 pA, –50 pA, 0 pA and +50 pA were applied at the soma prior to a 200 ms-long depolarizing (+200 pA) pulse to elicit one or more action potentials. If a spike occurred prior to the +200 pA pulse the trial was discarded. Protocols were repeated 30 times, before and after perfusion of 20 nM DTx-K, allowing 90 seconds for equilibration, and the data are shown as averages of the repetitions. No differences in resting membrane potential, input resistance or spike height were observed between genotypes or when comparing recordings before and after DTx-K application.

Drugs and toxins

AMPA, NMDA, $GABA_A$ and $GABA_B$ receptors were routinely blocked with 10 μM 2,3-dihydroxy-6-nitro-7- sulfamoyl-benzo[f]quinoxaline-2,3-dione, 50 μM (2R)-amino-5-phosphonovaleric acid, 100 μM picrotoxin, and 1 μM CGP 52432. DTx-K (20 nM) was used to block Kv1.1 channels.

APV was from Ascent (UK). DTx-K and UK-78282 were from Alomone (UK). All other compounds were purchased from Tocris (Bristol).

Pure synaptosome preparation

Pure synaptosomes were prepared using protocols adapted from refs. (42, 43). Brain cortices from four wild type or four *Kcna1*$^{V408A/+}$ mice (6 – 8 weeks old) were homogenized in 10 volumes of ice-cold HEPES-buffered sucrose (320 mM sucrose, 4 mM HEPES, pH 7.4, protease inhibitor cocktail – Sigma S8830) using a motor driven glass-Teflon homogenizer at ~900 rpm with 15 gentle strokes. The homogenate was centrifuged at 1,000 g for 10 min at 4°C in a Ti 70.1 rotor (Beckman). The pellet (P1) was discarded and the supernatant (S1) was centrifuged at 10,000 g for 15 min in the same rotor. The resulting pellet (P2) was re-suspended in 10 volumes of HEPES-buffered sucrose and then re-spun at 10,000 g for a further 15 min to yield a washed crude synaptosomal fraction. The supernatant was removed and the synaptosome-enriched pellet (P2') was re-suspended in 4 ml of homogenization buffer. The P2' fraction was then layered onto 3 ml of 1.2 M sucrose (supplemented with 4 mM HEPES pH7.4, protease inhibitors), and centrifuged at 230,000 g for 15 min in an SW55 Ti swinging bucket rotor (Beckman). The synaptosomes were recovered at the interface of HEPES-buffered sucrose and 1.2 M sucrose, and diluted to 8 ml with ice-cold HEPES-buffered sucrose. The samples were then layered onto 4 ml of 0.8 M sucrose (supplemented with 4 mM HEPES pH7.4, protease inhibitors) and centrifuged at 230,000 g for 15 min in a Ti 70.1 rotor (Beckman). The resulting pellet containing pure synaptomes was re-suspended in lysis buffer (1% NP40, 50 mM Tris-HCl (pH 8), 150 mM NaCl, and 2 mM EDTA, protease inhibitor) and the protein concentration was then determined with a Bio-Rad protein assay solution with bovine serum albumin (BSA) as a standard.

Western blot analyses

Equal amounts of proteins (30 µg/lane) from pure synaptosomal fraction of wild type or *Kcna1*$^{V408A/+}$ KI mice were separated by SDS-PAGE using Bis-Tris gradient gels (4–12% NuPAGE, Invitrogen) according to the manufacturer's recommendations and electrophoretically transferred onto Immobilon-P transfer membranes (Millipore). Membranes were immunoblotted with the respective antibodies: rabbit anti-Kv1.1 (APC-161, Alamone Lab, 1:800), anti-Kv1.2 (APC-010, 1:1500), anti-Kv1.3 (APC-101, 1:1000), anti-Kv1.4 (APC-167, 1:500), anti-Kv1.6 (APC-003, 1:2000), and anti-SNAP25 (Abcam ab5666, 1:2000) at 4°C overnight. Blots were then exposed to horseradish peroxidase-conjugated goat anti-rabbit IgG (17210, Bio-Rad Laboratories, 1:5000) for 1 hour at room temperature. Blots were developed using ECL-Prime (GE Healthcare), visualized via a ChemiDoc™ Touch Imaging System, and analysed using Image Lab 5.2 software (Bio-Rab Laboratories). For the quantifications, the signal intensity of each of the Kv1 bands was normalized to the signal intensity of the corresponding SNAP25 bands, and then the *Kcna1*$^{V408A/+}$ synaptosomes were expressed as a percentage of wild type.

Acknowledgements

We are indebted to J. Maylie for the gift of the *Kcna1* $^{V408A/+}$ mice, to S. Martin for help with breeding and genotyping, to M. Cano, E. Tagliatti and A. Vicente for preparation of neuronal cultures, and to members of the Experimental Epilepsy Group for helpful comments. This work was supported by the Medical Research Council, European Research Council and Wellcome Trust.

References

1. Alle H, Geiger JRP (2006) Combined analog and action potential coding in hippocampal mossy fibers. *Science* 311(5765):1290–1293.

2. Shu Y, Hasenstaub A, Duque A, Yu Y, McCormick DA (2006) Modulation of intracortical synaptic potentials by presynaptic somatic membrane potential. *Nature* 441(7094):761–765.

3. Scott R, Ruiz A, Henneberger C, Kullmann DM, Rusakov DA (2008) Analog modulation of mossy fiber transmission is uncoupled from changes in presynaptic Ca2+. *J Neurosci Off J Soc Neurosci* 28(31):7765–73.

4. Debanne D, Bialowas A, Rama S (2013) What are the mechanisms for analogue and digital signalling in the brain? *Nat Rev Neurosci* 14(1):63–69.

5. Christie JM, Chiu DN, Jahr CE (2011) Ca(2+)-dependent enhancement of release by subthreshold somatic depolarization. *Nat Neurosci* 14(1):62–68.

6. Kim S (2014) Action Potential Modulation in CA1 Pyramidal Neuron Axons Facilitates OLM Interneuron Activation in Recurrent Inhibitory Microcircuits of Rat Hippocampus. *PLOS ONE* 9(11):e113124.

7. Bialowas A, et al. (2015) Analog modulation of spike-evoked transmission in CA3 circuits is determined by axonal Kv1.1 channels in a time-dependent manner. *Eur J Neurosci* 41(3):293–304.

8. Shu Y, Yu Y, Yang J, McCormick DA (2007) Selective control of cortical axonal spikes by a slowly inactivating K+ current. *Proc Natl Acad Sci U S A* 104(27):11453–11458.

9. Kole MHP, Letzkus JJ, Stuart GJ (2007) Axon initial segment Kv1 channels control axonal action potential waveform and synaptic efficacy. *Neuron* 55(4):633–47.

10. Rall W (1959) Branching dendritic trees and motoneuron membrane resistivity. *Exp Neurol* 1(5):491–527.

11. Jackson MB (1993) Passive current flow and morphology in the terminal arborizations of the posterior pituitary. *J Neurophysiol* 69(3):692–702.

12. Ruiz A, Campanac E, Scott RS, Rusakov DA, Kullmann DM (2010) Presynaptic GABAA receptors enhance transmission and LTP induction at hippocampal mossy fiber synapses. *Nat Neurosci* 13(4):431–438.

13. Turecek R, Trussell LO (2001) Presynaptic glycine receptors enhance transmitter release at a mammalian central synapse. *Nature* 411(6837):587–590.

14. Awatramani GB, Price GD, Trussell LO (2005) Modulation of transmitter release by presynaptic resting potential and background calcium levels. *Neuron* 48(1):109–121.

15. Novak P, et al. (2009) Nanoscale live-cell imaging using hopping probe ion conductance microscopy. *Nat Methods* 6(4):279–281.

16. Novak P, et al. (2013) Nanoscale-targeted patch-clamp recordings of functional presynaptic ion channels. *Neuron* 79(6):1067–1077.

17. Lorincz A, Nusser Z (2008) Cell-type-dependent molecular composition of the axon initial segment. *J Neurosci Off J Soc Neurosci* 28(53):14329–14340.

18. Stühmer W, et al. (1989) Molecular basis of functional diversity of voltage-gated potassium channels in mammalian brain. *EMBO J* 8(11):3235–3244.

19. Grissmer S, et al. (1994) Pharmacological characterization of five cloned voltage-gated K+ channels, types Kv1.1, 1.2, 1.3, 1.5, and 3.1, stably expressed in mammalian cell lines. *Mol Pharmacol* 45(6):1227–34.

20. Wang H, Kunkel DD, Schwartzkroin PA, Tempel BL (1994) Localization of Kv1.1 and Kv1.2, two K channel proteins, to synaptic terminals, somata, and dendrites in the mouse brain. *J Neurosci Off J Soc Neurosci* 14(8):4588–4599.

21. Veh RW, et al. (1995) Immunohistochemical Localization of Five Members of the KV1 Channel Subunits: Contrasting Subcellular Locations and Neuron-specific Co-localizations in Rat Brain. *Eur J Neurosci* 7(11):2189–2205.

22. Harvey AL, Robertson B (2004) Dendrotoxins: Structure-Activity Relationships and Effects on Potassium Ion Channels. *Curr Med Chem* 11(23):3065–72.

23. Smart SL, et al. (1998) Deletion of the K(V)1.1 potassium channel causes epilepsy in mice. *Neuron* 20(4):809–19.

24. Browne DL, et al. (1994) Episodic ataxia/myokymia syndrome is associated with point mutations in the human potassium channel gene, KCNA1. *Nat Genet* 8(2):136–40.

25. Rajakulendran S, Schorge S, Kullmann DM, Hanna MG (2007) Episodic ataxia type 1: a neuronal potassium channelopathy. *Neurother J Am Soc Exp Neurother* 4(2):258–66.

26. Zerr P, Adelman JP, Maylie J (1998) Episodic ataxia mutations in Kv1.1 alter potassium channel function by dominant negative effects or haploinsufficiency. *J Neurosci Off J Soc Neurosci* 18(8):2842–8.

27. Zuberi SM, et al. (1999) A novel mutation in the human voltage-gated potassium channel gene (Kv1.1) associates with episodic ataxia type 1 and sometimes with partial epilepsy. *Brain J Neurol* 122 (Pt 5):817–25.

28. Adelman JP, Bond CT, Pessia M, Maylie J (1995) Episodic ataxia results from voltage-dependent potassium channels with altered functions. *Neuron* 15(6):1449–54.

29. Herson PS, et al. (2003) A mouse model of episodic ataxia type-1. *Nat Neurosci* 6(4):378–83.

30. Hanson DC, et al. (1999) UK-78,282, a novel piperidine compound that potently blocks the Kv1.3 voltage-gated potassium channel and inhibits human T cell activation. *Br J Pharmacol* 126(8):1707–1716.

31. Geiger JR, Jonas P (2000) Dynamic control of presynaptic Ca(2+) inflow by fast-inactivating K(+) channels in hippocampal mossy fiber boutons. *Neuron* 28(3):927–39.

32. Begum R, Bakiri Y, Volynski KE, Kullmann DM (2016) Action potential broadening in a presynaptic channelopathy. *Nat Commun* in press.

33. Bucurenciu I, Kulik A, Schwaller B, Frotscher M, Jonas P (2008) Nanodomain coupling between Ca2+ channels and Ca2+ sensors promotes fast and efficient transmitter release at a cortical GABAergic synapse. *Neuron* 57(4):536–545.

34. Ermolyuk YS, et al. (2012) Independent regulation of Basal neurotransmitter release efficacy by variable Ca^2+ influx and bouton size at small central synapses. *PLoS Biol* 10(9):e1001396.

35. D'Adamo MC, Liu Z, Adelman JP, Maylie J, Pessia M (1998) Episodic ataxia type-1 mutations in the hKv1.1 cytoplasmic pore region alter the gating properties of the channel. *EMBO J* 17(5):1200–7.

36. Imbrici P, D'Adamo MC, Grottesi A, Biscarini A, Pessia M (2011) Episodic ataxia type 1 mutations affect fast inactivation of K+ channels by a reduction in either subunit surface expression or affinity for inactivation domain. *Am J Physiol Cell Physiol* 300(6):C1314-1322.

37. Rea R, Spauschus A, Eunson LH, Hanna MG, Kullmann DM (2002) Variable K(+) channel subunit dysfunction in inherited mutations of KCNA1. *J Physiol* 538(Pt 1):5–23.

38. Maylie B, Bissonnette E, Virk M, Adelman JP, Maylie JG (2002) Episodic ataxia type 1 mutations in the human Kv1.1 potassium channel alter hKvbeta 1-induced N-type inactivation. *J Neurosci Off J Soc Neurosci* 22(12):4786–93.

39. Apostolides PF, Milstein AD, Grienberger C, Bittner KC, Magee JC (2016) Axonal Filtering Allows Reliable Output during Dendritic Plateau-Driven Complex Spiking in CA1 Neurons. *Neuron* 89(4):770–783.

40. Brunetti O, et al. (2012) Kv1.1 knock-in ataxic mice exhibit spontaneous myokymic activity exacerbated by fatigue, ischemia and low temperature. *Neurobiol Dis* 47(3):310–321.

41. Wang H, Kunkel DD, Martin TM, Schwartzkroin PA, Tempel BL (1993) Heteromultimeric K+ channels in terminal and juxtaparanodal regions of neurons. *Nature* 365(6441):75–9.

42. Hebb CO, Whittaker VP (1958) Intracellular distributions of acetylcholine and choline acetylase. *J Physiol* 142(1):187–196.

43. Bai F, Witzmann FA (2007) Synaptosome proteomics. *Subcell Biochem* 43:77–98.

Figure Legends

Fig. 1. Dual recordings from the soma and small presynaptic bouton of the same neuron. **(A)** Transmitted light image of a neuron with somatic patch pipette, with a neighboring 6 µm x 6 µm region selected for HPICM indicated with the square. **(B)** Left, Schematics indicating HPICM in voltage clamp mode (top) and whole-cell recording from presynaptic bouton (bottom). Right, height-coded image corresponding to highlighted area in (a), showing bouton (arrow) supplied by an axon adjacent to a dendrite. **(C)** Simultaneous somatic and presynaptic recordings of action potential train elicited by somatic current injection from the same cell as in (A). **(D)** Epifluorescence image (top) and overlaid epifluorescence image on the transmitted light image, showing neighboring boutons supplied by the same axon filled with Alexa Fluor 568 in the bouton pipette (after pipette withdrawal). The axon runs approximately horizontally through the image but typically could not be traced back to the soma. Scale bars: (A) 20 µm, (B) 1 µm, and (D) 20 µm.

Fig. 2. Kv1.1 channels determine spike width. (A) Example recordings from one neuron before and after 20 nM DTx-K application. This had no effect on somatic spikes but led to broadening of presynaptic action potentials**. (B)** Presynaptic spike widths elicited by somatic current injection before and after DTx-K perfusion, showing a significant broadening (n = 24 neurons, p<0.001, paired t-test). The diagonal line indicates no change. **(C)** Action potentials recorded from boutons, but not somata, of *Kcna1*$^{V408A/+}$ neurons were wider than in wild type neurons (WT: n = 29; *Kcna1*$^{V408A/+}$, n = 13; ***, p < 0.001, unpaired t-test). Spikes were also significantly narrower in boutons than somata in wild type (p < 0.05, paired t-test), but not *Kcna1*$^{V408A/+}$ neurons. **(D)** Example traces showing failure of DTx-K to broaden either somatic or presynaptic spikes in a *Kcna1*$^{V408A/+}$ neuron. **(E)** Summary data showing occlusion of

presynaptic spike broadening by DTx-K and *Kcna1*$^{V408A/+}$ (mean change: 1 ± 1%, *n* =12; *p* = 0.33). Scale bar in (A) and (D): 40 mV / 1ms.

Fig. 3. Blockade or deletion of Kv1.1 does not prevent analog modulation of presynaptic spike width. (A) Trace analysis from one wild type cell showing bidirectional changes in presynaptic spike width by subthreshold somatic current injections prior to evoking action potentials. **(A_1)** Superimposed spikes elicited after prepulses ranging between –100 pA and +50 pA. Each trace is shown in bold until after the first spike. Inset, experimental design showing somatic current injection protocol. **(A_2)** Zoomed presynaptic spikes obtained following –100 pA and +50 pA pre-pulses (asterisks in (A_1)). **(A_3)** Spike half-width plotted against somatic current injection showing positive dependence (half-width was ranked –50 pA < –100 pA < 0 pA < +50 pA, yielding Spearman rank correlation coefficient ρ = 0.8). **(A_4)** Half-width plotted against membrane potential measured at bouton prior to +200 pA somatic current injection to elicit spike. **(B)** Summary data obtained from wild type neurons before (*n* = 20, filled symbols) and after DTx-K (*n* = 18, open symbols), showing persistence of analog modulation of spike width. To compare among neurons spike half-widths recorded in individual experiments were normalized by the average width measured with –100 and –50 pA prepulses. **(C)** Genetic deletion of Kv1.1 also failed to abolish pre-pulse evoked spike broadening (*n* = 9; wild type data are replotted from (B) and shown in gray). Scale bar in (A): 40 mV / 1 ms.

Fig. 4. A heterozygous Episodic Ataxia mutation abolishes analog modulation of presynaptic spike width. (A) Absence of spike broadening in an example *Kcna1*$^{V408A/+}$ neuron. Data shown as in Fig. 3A. **(B)** Summary data from *Kcna1*$^{V408A/+}$ neurons (*n* = 10; open symbols)

superimposed on wild type data (gray). Error bars are in some cases smaller than the symbols.

**, $p < 0.01$ (*t*-test). Scale bar in (A): 40 mV / 1 ms.

Fig. 1

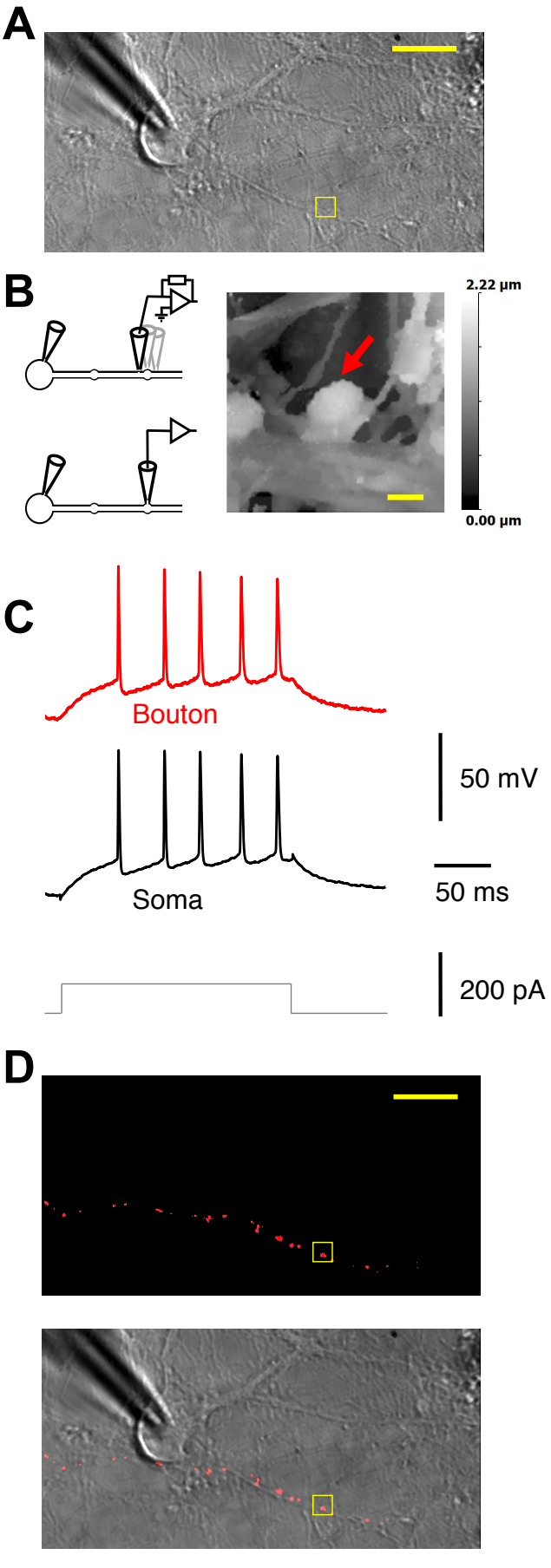

Fig. 2

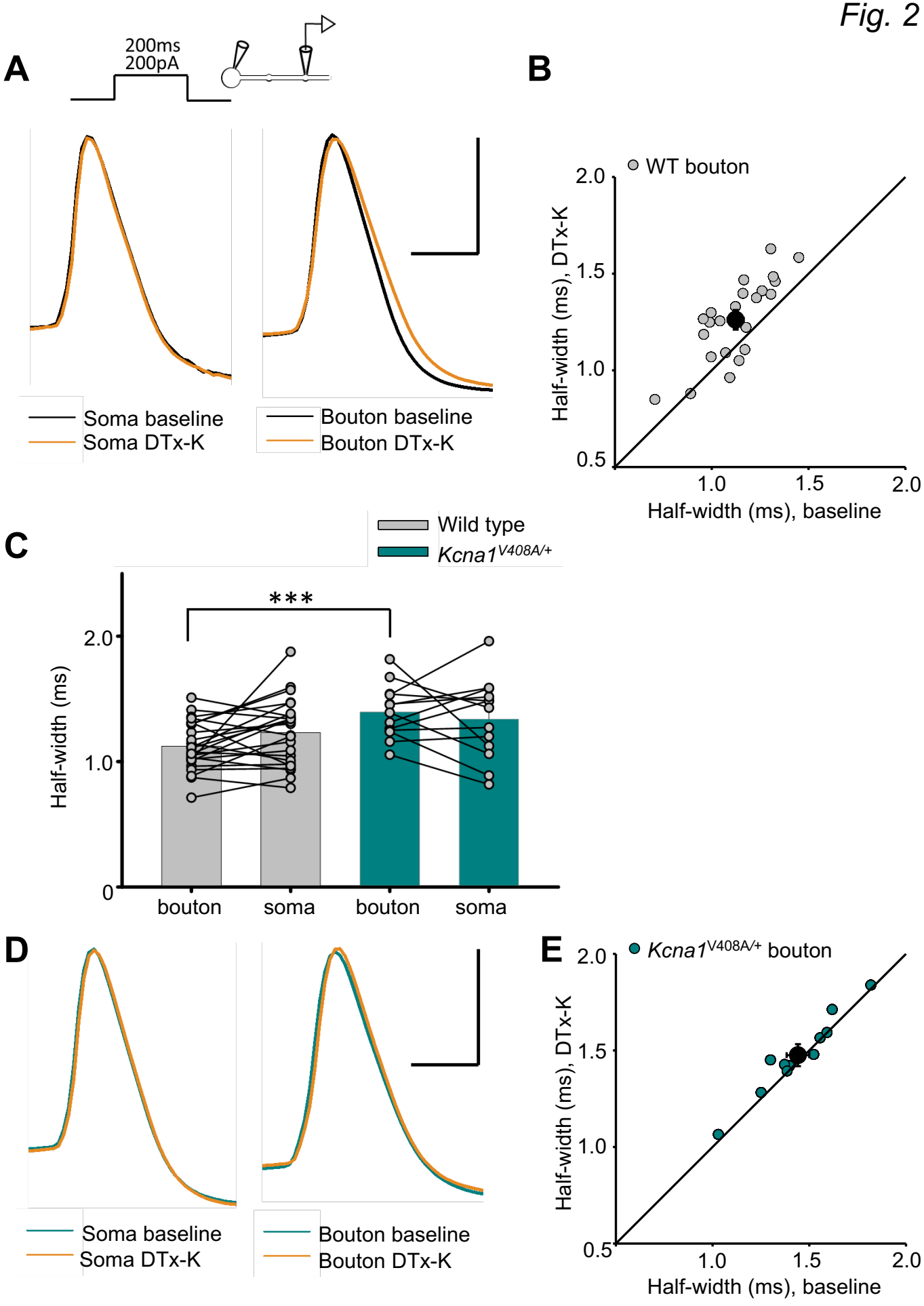
A
200ms
200pA
Soma baseline
Soma DTx-K
Bouton baseline
Bouton DTx-K
B
WT bouton
Half-width (ms), DTx-K
Half-width (ms), baseline
2.0
1.5
1.0
0.5
C
Wild type
Kcna1V408A/+
***
Half-width (ms)
2.0
1.0
0
bouton
soma
bouton
soma
D
Soma baseline
Soma DTx-K
Bouton baseline
Bouton DTx-K
E
Kcna1V408A/+ bouton
Half-width (ms), DTx-K
Half-width (ms), baseline
2.0
1.5
1.0
0.5

Fig. 3

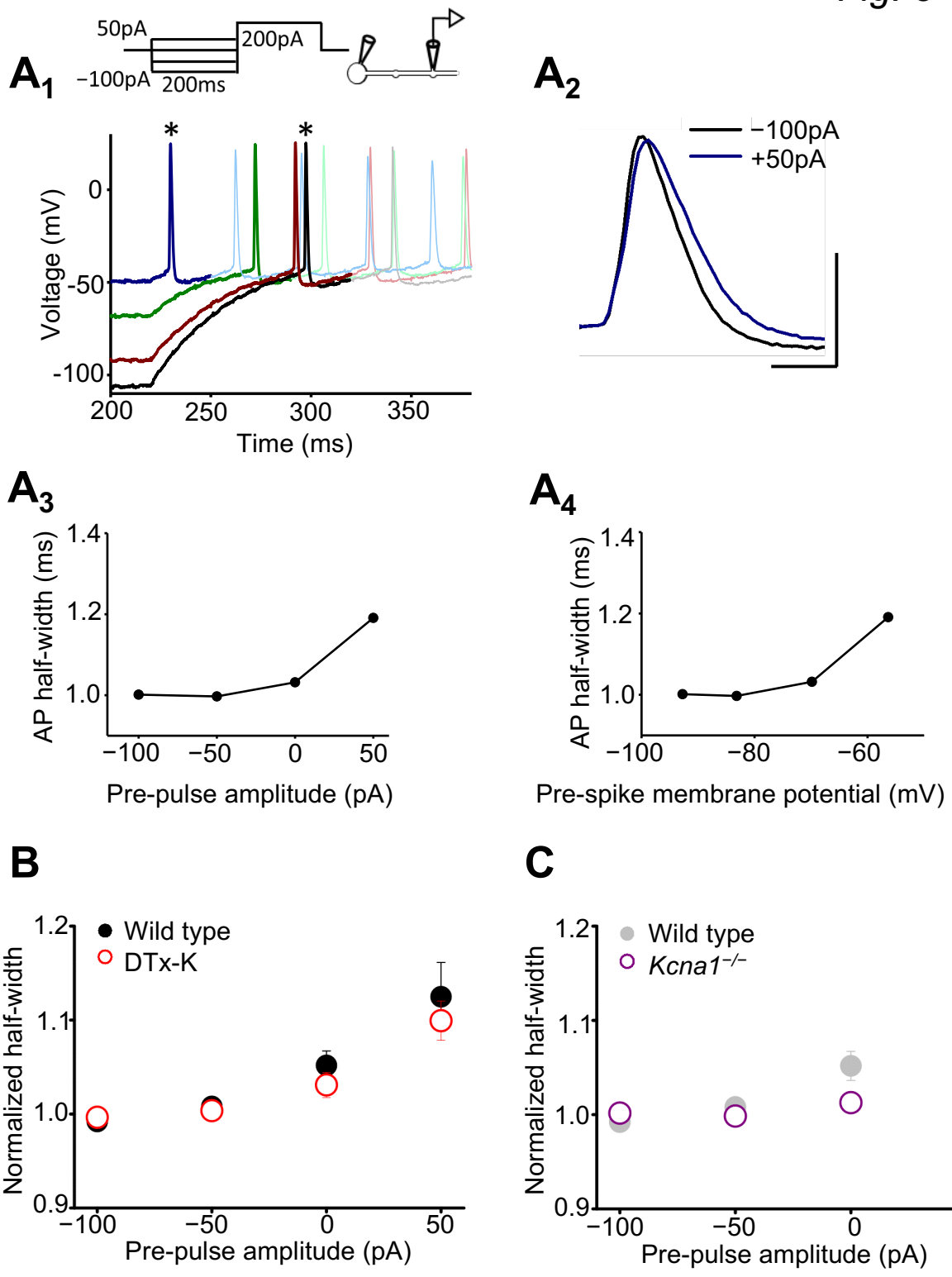
A1
50pA
200pA
−100pA
200ms
Voltage (mV)
0
-50
-100
200
250
300
350
Time (ms)
A2
−100pA
+50pA
A3
AP half-width (ms)
1.4
1.2
1.0
−100
−50
0
50
Pre-pulse amplitude (pA)
A4
AP half-width (ms)
1.4
1.2
1.0
−100
−80
−60
Pre-spike membrane potential (mV)
B
Wild type
DTx-K
Normalized half-width
1.2
1.1
1.0
0.9
−100
−50
0
50
Pre-pulse amplitude (pA)
C
Wild type
Kcna1−/−
Normalized half-width
1.2
1.1
1.0
0.9
−100
−50
0
50
Pre-pulse amplitude (pA)

Fig. 4

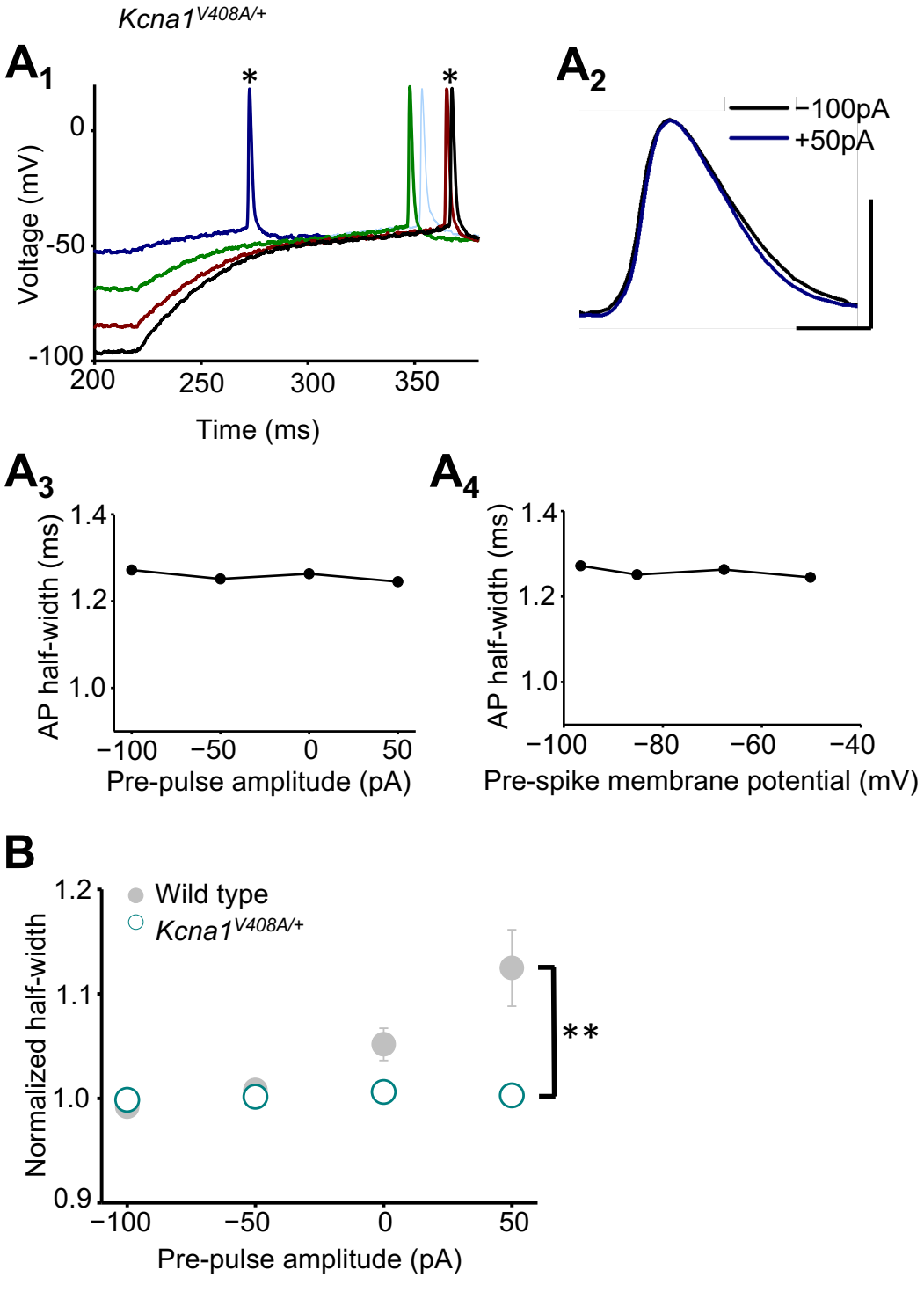
Kcna1V408A/+
A1
Voltage (mV)
0
-50
-100
200
250
300
350
Time (ms)
A2
−100pA
+50pA
A3
AP half-width (ms)
1.4
1.2
1.0
−100
−50
0
50
Pre-pulse amplitude (pA)
A4
AP half-width (ms)
1.4
1.2
1.0
−100
−80
−60
−40
Pre-spike membrane potential (mV)
B
Wild type
Kcna1V408A/+
Normalized half-width
1.2
1.1
1.0
0.9
−100
−50
0
50
Pre-pulse amplitude (pA)
**

Fig. S1. DTx-K had no effect on somatic spike half-width in wild type neurons. Mean change ± SEM: 1 ± 2%, n = 24 (p = 0.6, paired t-test).

Fig. S2. Genetic deletion of *Kcna1* broadened presynaptic spikes and occluded the effect of DTx-K. (**A**) Action potentials recorded from boutons, but not somata, of *Kcna1*$^{-/-}$ neurons (n = 9) were broader than in wild type neurons (replotted from Fig. 2C; **, $p < 0.01$, t-test). (**B**) Sample traces from one *Kcna1*$^{-/-}$ neuron showing simultaneously recorded somatic and presynaptic spikes before and after DTx-K application. Scale: 40 mV / 1 ms. (**C**) Summary data showing partial occlusion of presynaptic spike broadening by DTx-K in *Kcna1*$^{-/-}$ neurons (mean change: 4 ± 2%, n = 7, p = 0.05, paired t-test). (**D**) Summary data showing absence of somatic spike broadening by DTx-K (mean change: 1 ± 1 %; p = 0.77, paired t-test).

Fig. S3. DTx-K had no effect on somatic spike half-width in *Kcna1*$^{V408A/+}$ neurons. Mean change: 0 ± 2% (n = 12; p = 0.75, paired t-test).

Fig. S4. Effect of DTx-K on spikes elicited at the bouton, without simultaneous somatic recordings. (**A**) Recordings from wild type neurons. Left, sample traces before and after 20 nM DTx-K application. Right, presynaptic spike widths in 24 neurons before and after DTx-K perfusion, showing 18 ± 3 % broadening (n = 23, p<0.001, paired t-test). Inset, schematic showing current injection into the recoded bouton. (**B**) Recordings from *Kcna1*$^{-/-}$ neurons. Left, sample traces from one neuron before and after DTx-K application. Right, DTx-K failed to broaden bouton spike width in *Kcna1*$^{-/-}$ neurons (2 ± 1%, n = 7; p = 0.09, paired t-test). (**C**) Recordings from *Kcna1*$^{V408A/+}$ neurons. Left, sample traces before and after DTx-K. Right, DTx-K

had no effect on bouton spike width in *Kcna1*$^{V408A/+}$ neurons (2 ± 1%, n = 8; p = 0.09). Scale bar in (A) applies to (B) and (C): 40 mV / 2 ms.

Fig. S5. Analogue spike width modulation in WT and *Kcna1*$^{V408A/+}$ neurons. (**A**) Top, spike width dependence on somatic pre-pulse current shown for individual WT neurons. Bottom, corresponding distribution of Spearman rank correlation coefficients (ρ) demonstrating prevalence of cells that show a positive relationship between the spike half-width and the pre-pulse (n = 20, p < 0.005, Wilcoxon signed rank test). (**B**) Top, spike width dependence on somatic pre-pulse current shown for individual *Kcna1*$^{V408A/+}$ neurons. Bottom, corresponding distribution of Spearman rank correlation coefficients (ρ) showing now systematic relationship between half-width and pre-pulse (n = 10, p < 0.8, Wilcoxon signed rank test, p < 0.02, Mann-Whitney U test comparing to WT).

Fig. S6. Subthreshold modulation of spike width is unaffected by the Kv1.3 and Kv1.4 blocker UK-78282. Data plotted as for Fig. 3B (n = 5).

Fig. S7. Subthreshold modulation of spike width in a *Kcna1*$^{-/-}$ neuron. (**A**) Sample traces showing spikes evoked by somatic +200 pA current injection following subthreshold somatic prepulses. Each trace is shown in bold until after the first spike. The spikes evoked following –100 pA and +50 pA prepulses (asterisks) are expanded at right. Scale bar: 40 mV / 1 ms. (**B**) Spike half-width plotted against somatic current injection showing positive dependence. (**C**) Half-width plotted against the membrane potential measured at the bouton prior to the +200 pA somatic current injection used to elicit spike.

Fig. S8. Subthreshold modulation of spike width for *Kcna1*$^{V408A/+}$ and wild type littermates. Data plotted as in Fig. 3C (error bars for *Kcna1*$^{V408A/+}$ are smaller than the symbols). **, $p < 0.01$ (WT n = 11, *Kcna1*$^{V408A/+}$ n = 10, *t*-test).

Fig. S9. Subthreshold modulation of spike width using longer pre-pulses. Data plotted as in Fig. 3C. Pre-pulses lasted 2 seconds. **, $p < 0.01$ (WT n = 5, *Kcna1*$^{V408A/+}$ n = 5, *t*-test).

Fig. S10. Kv1 subunit expression in cortical synaptosomes from wild type and *Kcna1*$^{V408A/+}$ mice.

(**A**) Representative immunoblots of Kv1 subunits in synaptosome preparations from wild type (WT) and *Kcna1*$^{V408A/+}$ mice (*Kcna1*$^{V408A/+}$). Top panels: immunostaining with subunit-specific anti-Kv1 antibodies (Abs); bottom panels: loading control, immunostaining with anti-SNAP25 Ab. Molecular weight protein markers (kDa) are shown on the left of each blot. (**B**) Quantification. Specific immunoreactive signals for Kv1 subunits in *Kcna1*$^{V408A/+}$ synaptosomes in each lane (integral band intensity) were normalized to the corresponding SNAP25 band intensity and then expressed as a percentage of the corresponding WT preparation. Data are mean (±SEM) from 3 independent synaptosomal preparations from 4 WT and 4 *Kcna1*$^{V408A/+}$ mice.

Fig. S1

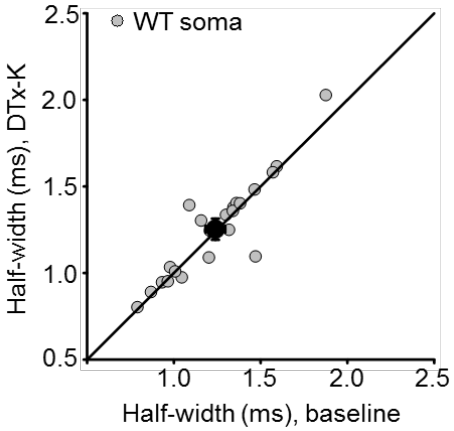
WT soma
Half-width (ms), DTx-K
Half-width (ms), baseline
2.5
2.0
1.5
1.0
0.5
1.0
1.5
2.0
2.5

Fig. S2

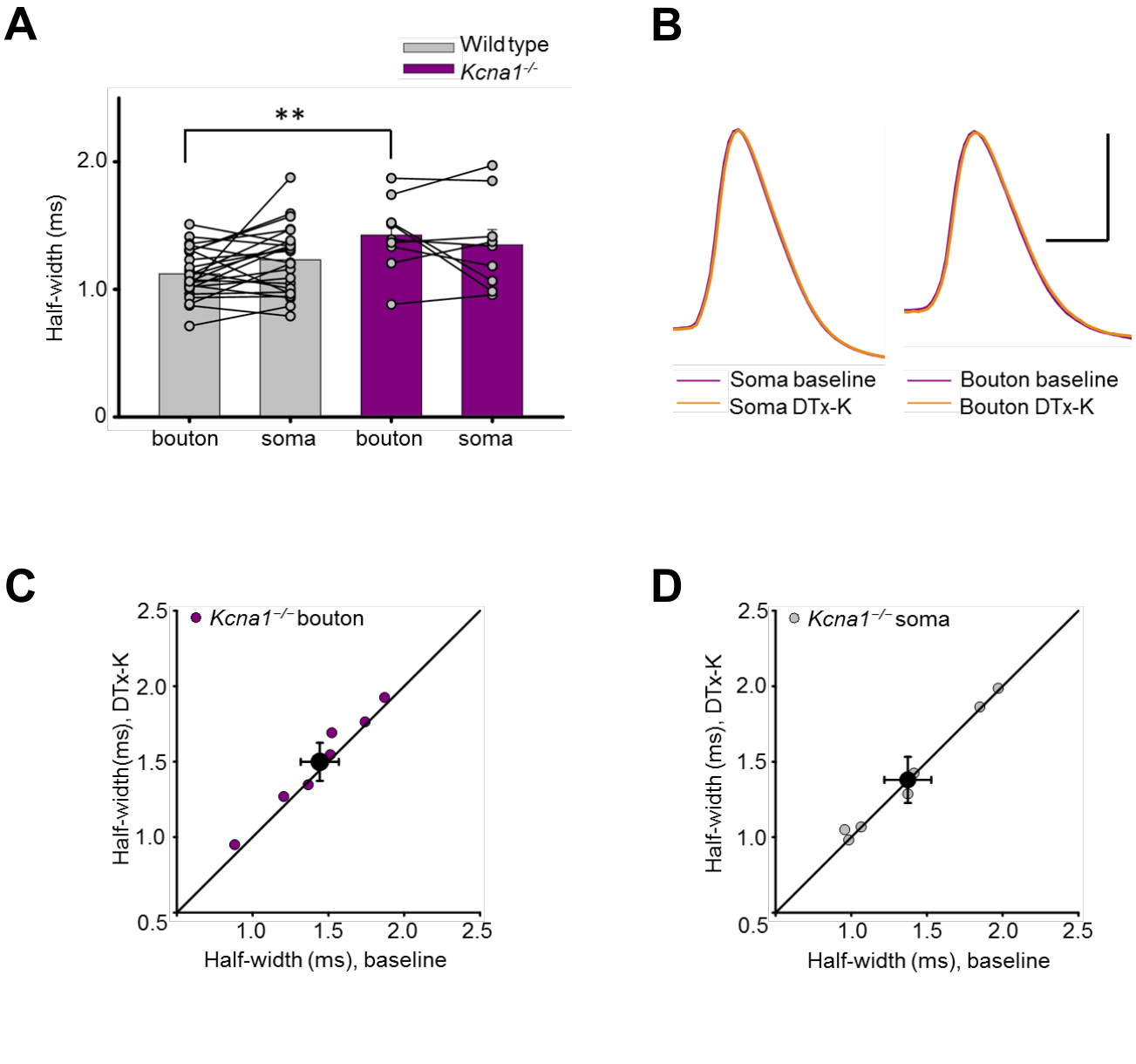
A
Wild type
Kcna1-/-
**
Half-width (ms)
2.0
1.0
0
bouton
soma
bouton
soma
B
Soma baseline
Soma DTx-K
Bouton baseline
Bouton DTx-K
C
Kcna1-/- bouton
Half-width(ms), DTx-K
2.5
2.0
1.5
1.0
0.5
1.0
1.5
2.0
2.5
Half-width (ms), baseline
D
Kcna1-/- soma
Half-width (ms), DTx-K
2.5
2.0
1.5
1.0
0.5
1.0
1.5
2.0
2.5
Half-width (ms), baseline

Fig. S3

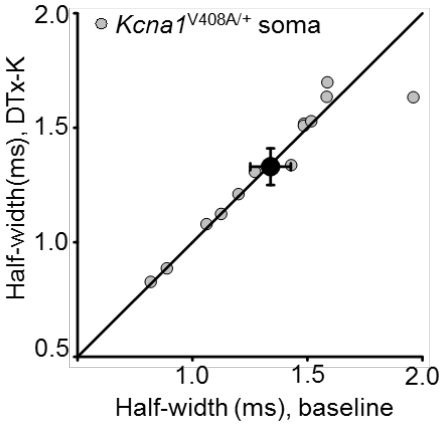
Kcna1V408A/+ soma
Half-width(ms), DTx-K
Half-width (ms), baseline
2.0
1.5
1.0
0.5
1.0
1.5
2.0

Fig. S4

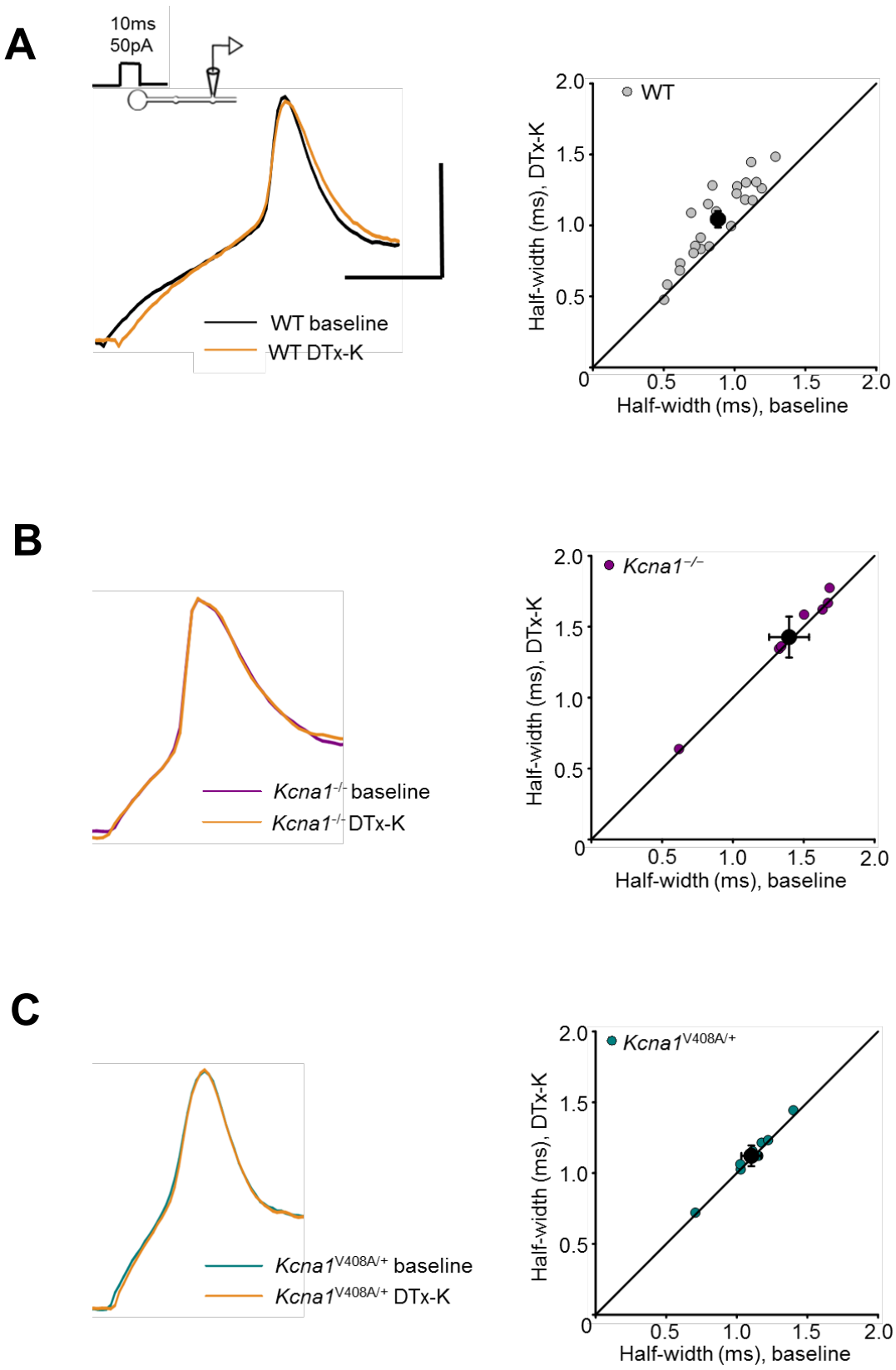
A
10ms
50pA
WT baseline
WT DTx-K
WT
Half-width (ms), DTx-K
Half-width (ms), baseline
B
Kcna1-/- baseline
Kcna1-/- DTx-K
Kcna1-/-
C
Kcna1V408A/+ baseline
Kcna1V408A/+ DTx-K
Kcna1V408A/+

Fig. S5

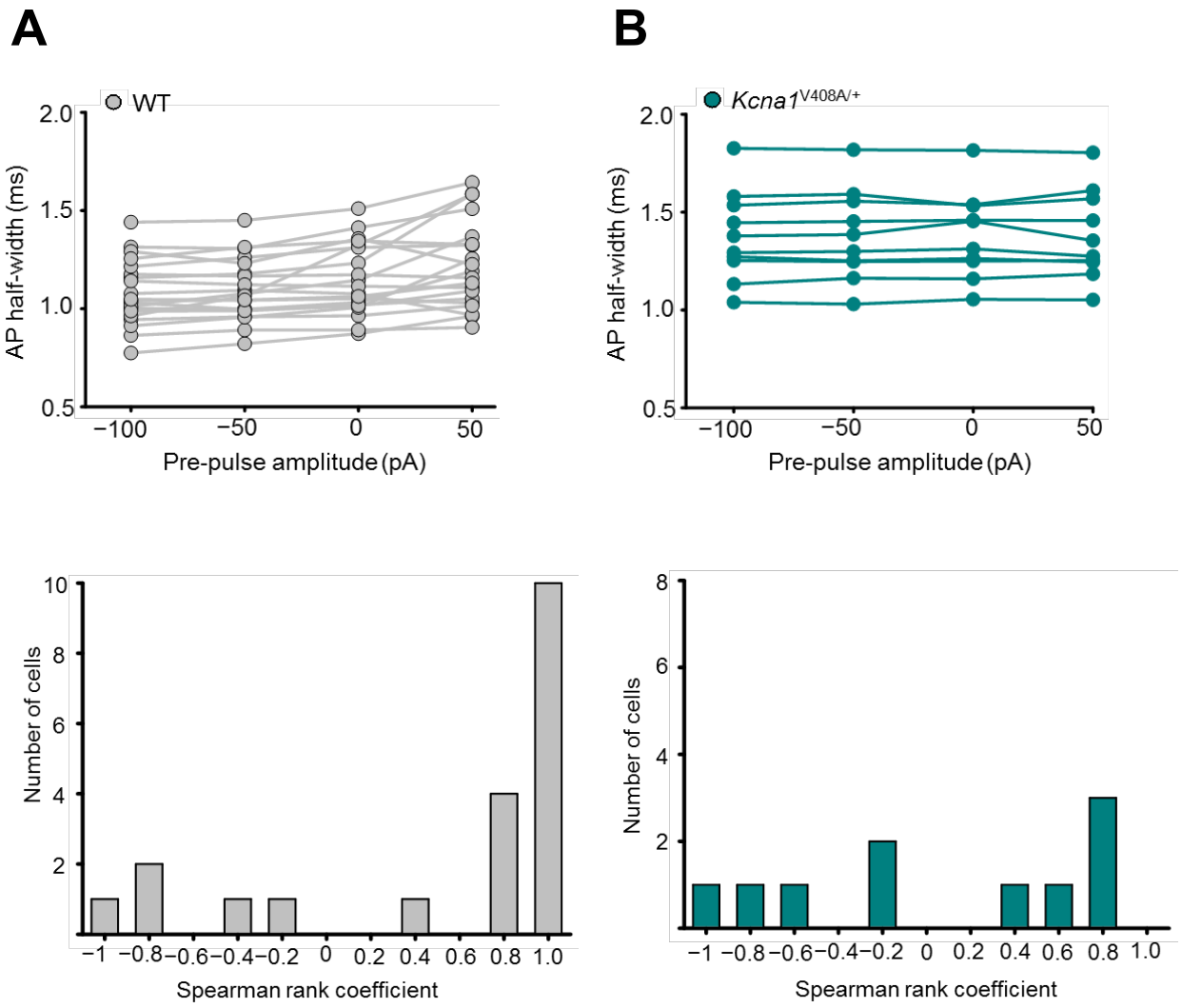
A
B
WT
Kcna1V408A/+
AP half-width (ms)
Pre-pulse amplitude (pA)
Number of cells
Spearman rank coefficient

Fig. S6

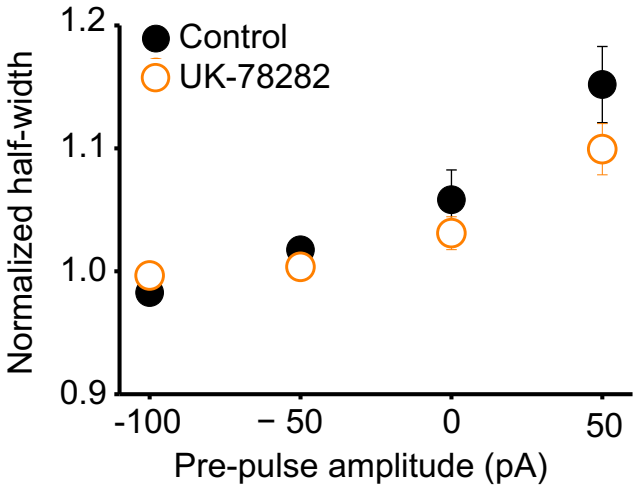
1.2
1.1
1.0
0.9
Normalized half-width
Control
UK-78282
-100
− 50
0
50
Pre-pulse amplitude (pA)

Fig. S7

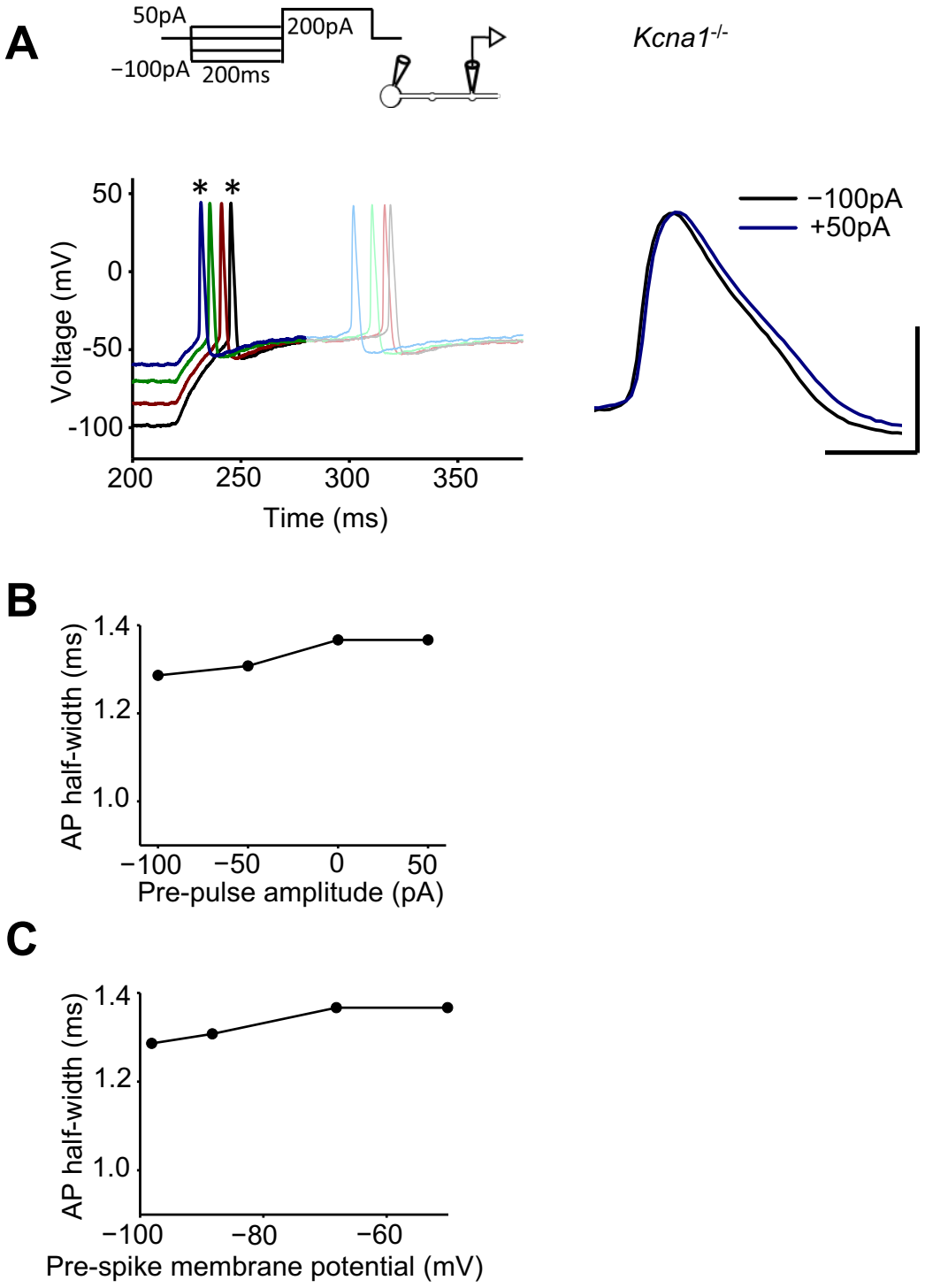
A
50pA
200pA
−100pA
200ms
Kcna1-/-
50
0
-50
-100
Voltage (mV)
200
250
300
350
Time (ms)
−100pA
+50pA
B
AP half-width (ms)
1.4
1.2
1.0
−100
−50
0
50
Pre-pulse amplitude (pA)
C
AP half-width (ms)
1.4
1.2
1.0
−100
−80
−60
Pre-spike membrane potential (mV)

Fig. S8

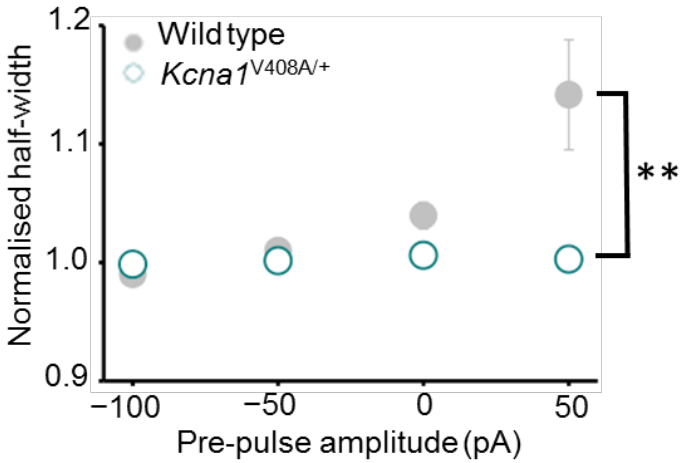
1.2
1.1
1.0
0.9
Normalised half-width
Wild type
Kcna1V408A/+
**
−100
−50
0
50
Pre-pulse amplitude (pA)

Fig. S9

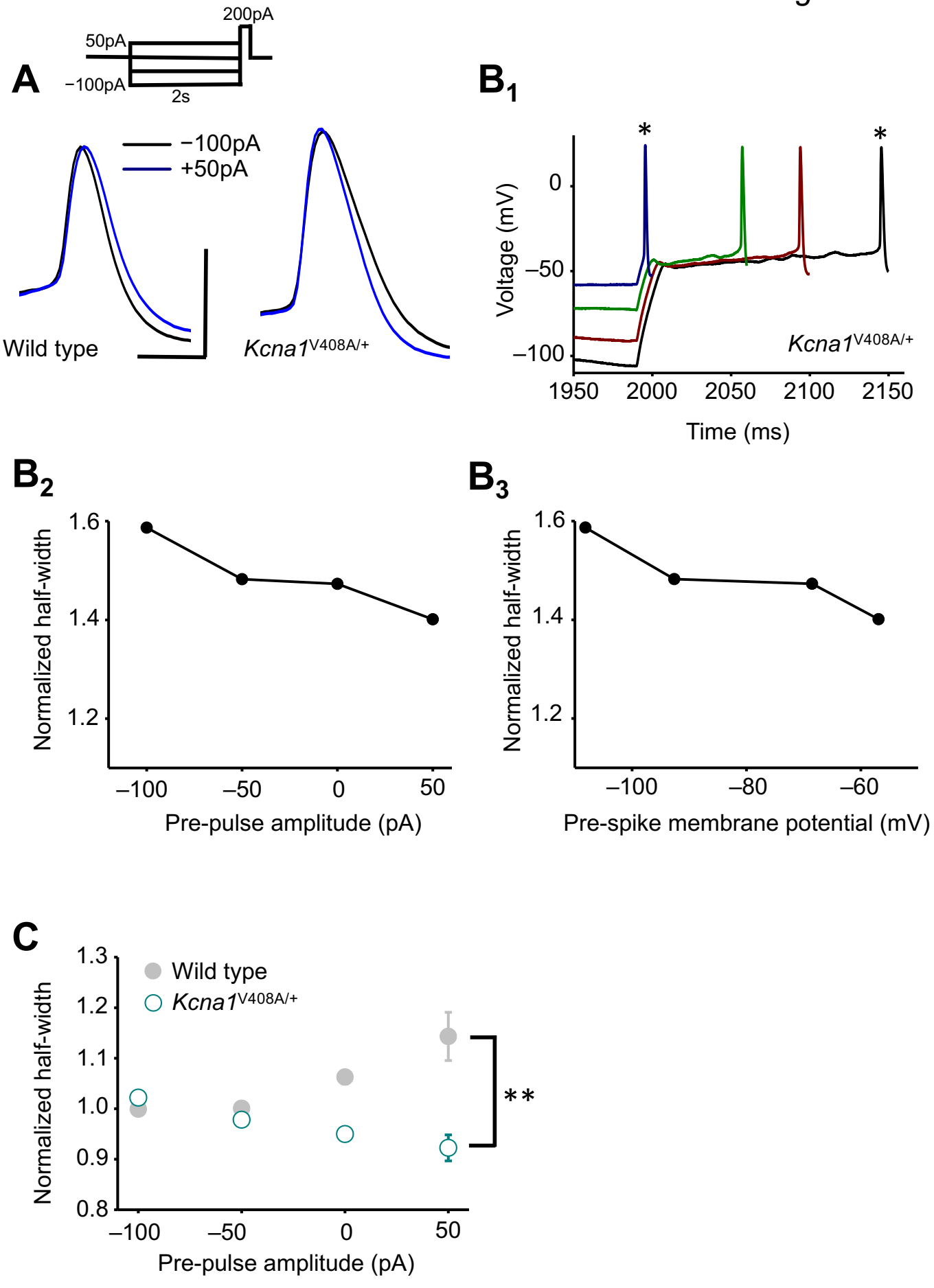
A
200pA
50pA
−100pA
2s
−100pA
+50pA
Wild type
Kcna1V408A/+
B1
Voltage (mV)
0
−50
−100
1950
2000
2050
2100
2150
Time (ms)
Kcna1V408A/+
B2
Normalized half-width
1.6
1.4
1.2
−100
−50
0
50
Pre-pulse amplitude (pA)
B3
Normalized half-width
1.6
1.4
1.2
−100
−80
−60
Pre-spike membrane potential (mV)
C
Normalized half-width
1.3
1.2
1.1
1.0
0.9
0.8
Wild type
Kcna1V408A/+
**
−100
−50
0
50
Pre-pulse amplitude (pA)

Fig. S10

A

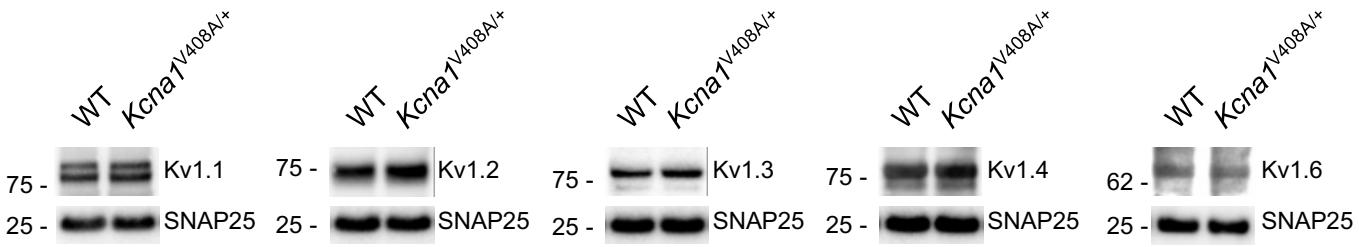
WT
Kcna1V408A/+
75 -
Kv1.1
25 -
SNAP25
75 -
Kv1.2
25 -
SNAP25
75 -
Kv1.3
25 -
SNAP25
75 -
Kv1.4
25 -
SNAP25
62 -
Kv1.6
25 -
SNAP25

B

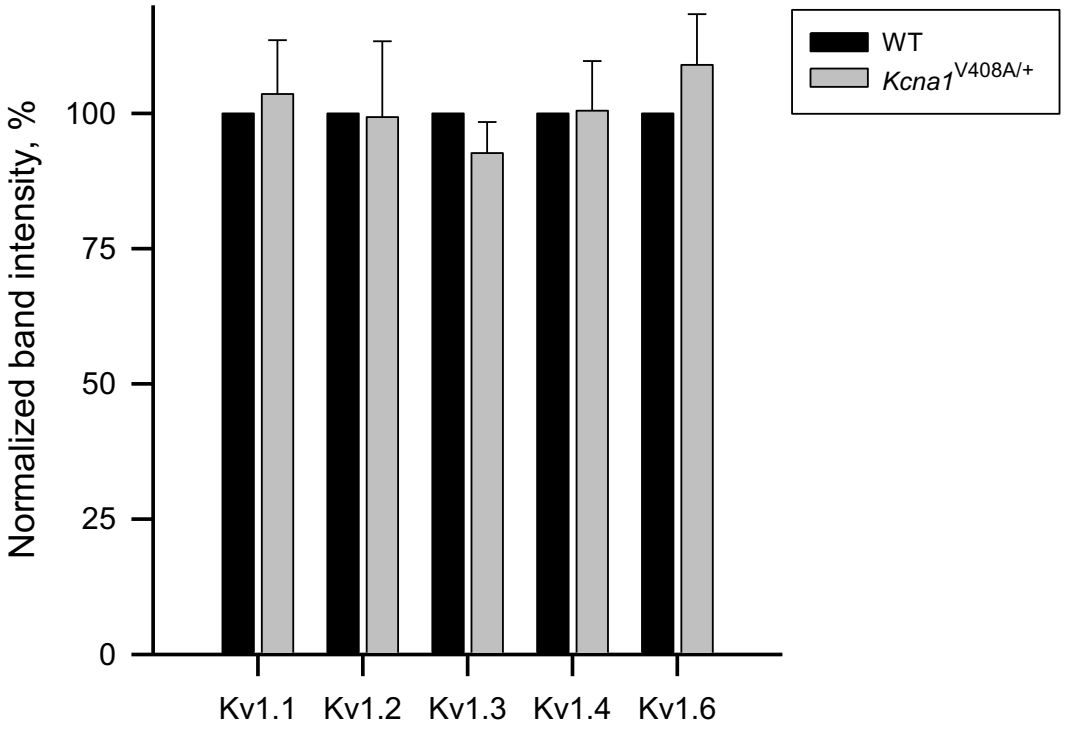
WT
Kcna1V408A/+
Normalized band intensity, %
100
75
50
25
0
Kv1.1
Kv1.2
Kv1.3
Kv1.4
Kv1.6